Formation and luminescence of ZnO nanoparticles embedded in MgO films

J. G. Ma
Key Laboratory of Excited State Processes, Changchun Institute of Optics, Fine Mechanics and Physics, Chinese Academy of Sciences, 16 East-south Lake Avenue, Changchun 130033, China

Y. C. Liu* and C. L. Shao
Center for Advanced Optoelectronic Functional Material Research, Northeast Normal University, Changchun 130024, China

J. Y. Zhang, Y. M. Lu, D. Z. Shen, and X. W. Fan
Key Laboratory of Excited State Processes, Changchun Institute of Optics, Fine Mechanics and Physics, Chinese Academy of Sciences, 16 East-south Lake Avenue, Changchun 130033, China

(Received 9 August 2004; revised manuscript received 15 November 2004; published 30 March 2005)

ZnO nanoparticles embedded in MgO thin films were prepared by a simple coevaporation method, and the subsequent thermal annealing in oxygen ambient at 300–1100 °C. X-ray diffraction and optical absorption spectra revealed that the size of ZnO nanoparticles embedded in MgO decreased with increasing annealing temperature, and MgZnO interlayers were formed between ZnO nanoparticles and MgO matrix. Analysis of Raman scattering spectra showed that the strain originated from lattice mismatch between ZnO and MgO was relaxed by annealing processes, and the MgZnO alloy layers between ZnO nanoparticles and MgO matrix were formed. In photoluminescence spectra, the exciton emissions of ZnO nanoparticles shift to shorter wavelengths with increasing annealing temperature. When the annealing temperatures exceeded 700 °C, a strong emission appeared at 3.58 eV, while the deep level emission band in the visible light region was dramatically quenched.

DOI: 10.1103/PhysRevB.71.125430 PACS number(s): 78.67.Bf, 78.55.Et, 81.15.Ef, 68.65.Hb

I. INTRODUCTION

Over the past few years, wide band gap semiconductors such as ZnSe, GaN, and ZnO have attracted much attention because of their potential applications for optoelectronic devices in the blue and ultraviolet (UV) spectral regions.[1–3] Among these materials, ZnO has been recognized as a promising candidate for the development of short-wavelength optical devices such as ultraviolet detectors, light-emitting diodes, and laser diodes. In terms of crystal structure, band gap, and optical properties, ZnO is quite similar to GaN. However, a pronounced advantage for ZnO is its large exciton binding energy, 60 meV,[4] a value more than twice that of GaN. This large exciton binding energy ensures significant excitonic emission at room temperature or even higher temperatures; so far, exciton-related optically pumped laser action in ZnO epitaxial films has been observed at room temperature.[5,6] Additionally, ZnO can be alloyed with MgO (E_g=7.8 eV) (Refs. [7,8]) or CdO (E_g=2.4) (Ref. [9]) to fine-tune the band gap in the UV and blue light region, which is favorable for applications of ZnO and its related materials.[10–12] Recently, nanoscaled ZnO materials such as quantum wells, nanowires, and nanoparticles have attracted substantial interest in materials research because of their features and potential applications.[13–17] While many different chemical synthesis methods have been reported for preparing nanoscaled ZnO materials in various forms, it is difficult to keep such materials stable at higher temperature and realize the combination of such materials with silicon-based electronic materials. Another problem for nanoscaled materials, especially nanoparticles, is that the high ratio of surface area to volume can introduce significant surface-related defects which dramatically decrease the exciton emission efficiency. To solve this problem, many researchers have attempted to passivate the surface defects by capping or embedding ZnO nanoparticles with other materials,[18] an approach that was explored further in this work. Here, ZnO nanoparticles were embedded in MgO films by a simple coevaporation method with subsequent thermal annealing. The formation and the structural and optical properties of ZnO nanoparticles were investigated with x-ray diffraction (XRD), optical absorption, Raman scattering, and photoluminescence (PL) measurements.

II. EXPERIMENTS

ZnO nanoparticles embedded in MgO films were prepared using an electron beam (EB) evaporation and resistance evaporation combination system. A bulk-MgO crystal and highly pure metal zinc (5 N) were used as evaporation sources. The experimental procedure was as follows: First, a MgO buffer layer of 20 nm was deposited on the substrates by EB evaporation. Second, MgO and Zn were deposited simultaneously by EB and resistance evaporations (i.e., Zn was evaporated from a resistance evaporator while MgO was deposited by EB evaporation) in a 200-nm-thick layer. Third, a 20-nm-thick MgO cover layer was deposited. The deposition ratios of MgO and Zn are 40 and 10 nm/min, respectively. EB evaporation voltage and current were constant at 8 kV and 55 mA, respectively. Single-crystal silicon (100) and silica glass were used as substrates for different measurements. The distance between the substrates and the evaporation sources was approximately 30 cm. Before the evaporation, the substrates were cleaned by the standard

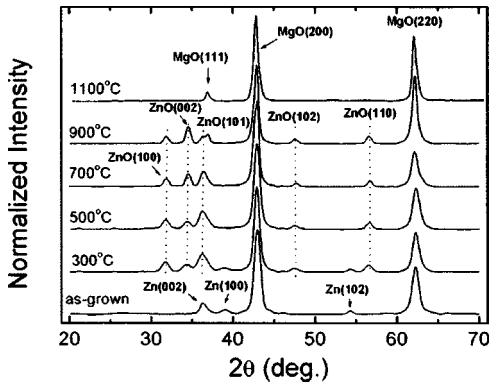

FIG. 1. X-ray diffraction spectra of the as-grown sample and the samples annealed at 300 °C–1100 °C.

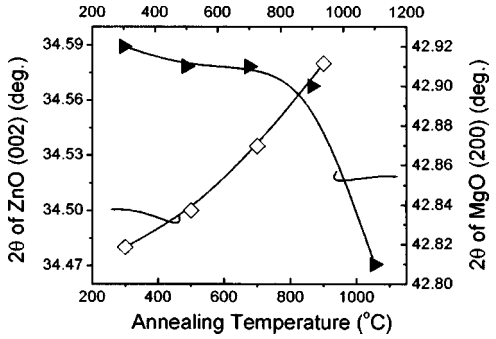

FIG. 2. Variation of the diffraction angles for ZnO (002) pattern and MgO (200) pattern with annealing temperature. Symbol (◇) corresponds to ZnO (002) pattern and symbol (▶) corresponds to MgO (200) pattern.

RCA clean processes,[19] then the evaporation system was evacuated to a base pressure below 5×10^{-4} Pa with a turbo molecular pump. During the deposition, the substrate temperature was maintained at 200 °C by a resistance heater. Finally, the samples were annealed in a standard diffusion furnace at a temperature of 300 °C, 500 °C, 700 °C, 900 °C, or 1100 °C for 1 h with an oxygen flux of 1 liter/min.

The structural characterizations of the samples were carried out by XRD using a D/max-RA x-ray spectrometer (Rigaku) with Cu Kα radiation of 1.54 Å. Optical absorption spectra were recorded using a Shimadzu UV-3101PC scanning spectrophotometer. Both PL and Raman spectra were collected with a JY-630 micro-Raman spectrometer made by the J-Y Company in France. The 325 nm line of a He-Cd laser was used as the excitation source.

III. RESULTS AND DISCUSSION

Figure 1 shows the $\theta-2\theta$ XRD spectra of the as-grown sample and those annealed at 300–1100 °C. The data have been normalized for easy comparison. All the samples show strong diffraction peaks corresponding to cubic MgO (200) and (220) patterns at $2\theta=42.92°$ and 62.3°, indicating that the samples consist mainly of MgO phase. For the as-grown sample (A), diffraction peaks appeared at $2\theta=36.3°$, 39.0°, and 54.3°, corresponding to the (002), (100), and (102) diffraction patterns of hexagonal zinc, respectively. Because of the strong MgO diffraction peaks, some Zn-related diffractions, such as the (101) peak, were obscured by MgO peaks. The average diameter of the Zn nanoparticles was approximately 15 nm, as estimated from the full width at half maximum (FWHM) of diffraction peaks by applying the Scherrer formula.[20] According to the experimental processes, it can be concluded that Zn nanoparticles had been embedded in MgO thin film in the as-grown sample. For the sample annealed at 300 °C, in addition to the diffraction peaks from the cubic MgO and the hexagonal Zn, several new diffraction peaks appeared at $2\theta=31.79°$, 34.43°, 35.3°, 47.57°, and 56.62°, respectively, corresponding to the (100), (002), (101), (102), and (110) diffraction patterns of hexagonal ZnO structure, respectively. This observation indicates that the Zn nanoparticles in MgO film were partially oxidized during annealing. Considering that course of oxidation from the surface to the interior of the Zn nanoparticles, smaller Zn nanoparticles will be transformed completely to ZnO after annealing, while larger nanoparticles will have Zn cores covered by a surface layer of ZnO. The thickness of the ZnO surface layer depends on annealing temperature. Thus, both ZnO and Zn diffraction peaks are observed in the XRD data. For the samples annealed at higher temperatures, the diffraction peaks of hexagonal ZnO become stronger, and the Zn-related diffraction peaks disappear, indicating the full oxidation of the Zn nanoparticles in MgO. Figure 2 shows the dependence of the XRD 2θ values corresponding to the maximum intensity of the ZnO (002) and MgO (200) peaks on the annealing temperature. As the annealing temperature increases, the diffraction angle of ZnO (002) shifts to the bigger angle side and the diffraction angle of MgO (200) shifts to the smaller angle side. The shift of XRD angle for the compositional variation of alloy is common in II-VI and III-VI ternary alloys.[10,21,22] Therefore, the shift of ZnO diffraction angles gives evidence of the formation of hexagonal phase MgZnO alloys in these samples. However, it is notable that the sample annealed at 1100 °C shows no diffraction peaks corresponding to ZnO or Zn, while the diffraction angle of the cubic MgO (200) peak shifts almost 0.1° to the low-angle side in comparison with the as-grown sample, as shown in Figs. 1 and 2. The reason for the shift of MgO (200) diffraction peaks may be due to the formation of cubic phase MgZnO alloys. This will be discussed further in the absorption spectra.

Absorption spectra for all samples are shown in Fig. 3. The optical band gap energy (E_g) of the samples can be calculated, assuming that ZnO nanoparticles obey the following allowed direct transition equation:[23] $\alpha=(A/h\nu)(h\nu-E_g)^{1/2}$, where α is the absorption coefficient, A is a constant, and $h\nu$ is photon energy. By plotting $(\alpha h\nu)^2$ vs $h\nu$ and extrapolating the linear portion to $\alpha=0$, the corresponding band gap energy can be obtained. For the as-grown sample only a very weak absorption can be observed. Using the equation above, the band gap energy is calculated to be 3.37 eV, which is similar to the band gap of ZnO bulk. Since it is inevitable that some zinc atoms would react with the residual oxygen molecular in the evaporation system or with the oxygen decomposed from MgO during sample growth,

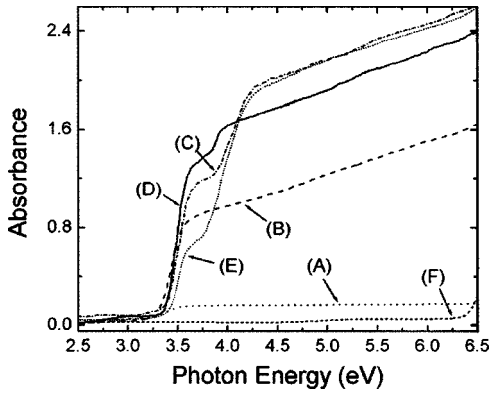

FIG. 3. Optical absorption spectra of the as-grown sample (A) and the samples annealed at temperatures of 300 °C (B), 500 °C (C), 700 °C (D), 900 °C (E), and 1100 °C (F).

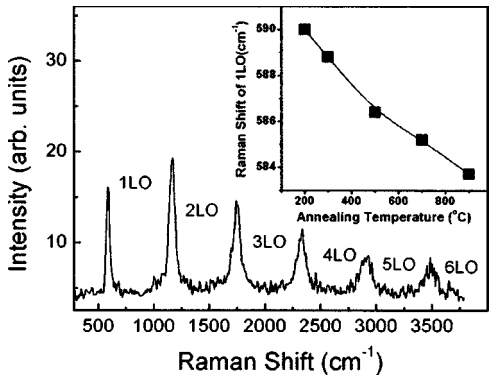

FIG. 4. Raman scattering spectrum of the sample annealed at 500 °C. The inset shows the dependence of 1-LO phonon frequency on annealing temperature, where the data point at 200 °C represents the as-grown sample.

the weak absorption at 3.37 eV can be attributed to the partially oxidized Zn nanoparticles. However, there are no ZnO-related diffraction patterns in the XRD spectrum. This is ascribed to the small amount and the poor quality of ZnO (i.e., ZnO may be amorphous) in the as-grown sample. For the samples annealed at 300 °C, an obvious absorption edge can be observed from which the band gap energy is calculated as 3.39 eV. As discussed in XRD analysis, Zn nanoparticles have been oxidized by annealing process. Therefore, the absorption for the sample annealed at 300 °C can be ascribed to ZnO nanoparticles embedded in MgO films. However, it is notable that the absorption spectra are composed of two absorption edges for the samples annealed at 500 °C, 700 °C, and 900 °C (Fig. 3). The absorptions at the low energy side are ascribed to the absorption of ZnO nanoparticles from which band gaps are calculated to be 3.42, 3.44, and 3.46 eV, respectively. In the same way, the band gap energies at the high energy side are calculated to be 3.63, 3.73, and 3.75 eV, respectively. As reported by others,[24–26] the band gap energy of hexagonal phase MgZnO alloys can be tuned from 3.37 to 4.1 eV by varying the Mg content. Consequently, the absorption at the high energy side observed in Fig. 3 contributes further evidence to the presence of hexagonal MgZnO alloys in MgO matrix. On the other hand, the band gap energies of ZnO nanoparticles and MgZnO alloys are both blueshifted while increasing annealing temperature, and the absorption coefficient at the low energy side decreases with increasing annealing temperature, whereas it increases at the high energy side. However, for the sample annealed at 1100 °C, the absorption edge starts at 6.4 eV, and it appears that the absorption at even higher energy may occur in this sample, which is out of range of the spectrometer used in this paper. It has been known that the band gap energy of MgO is 7.8 eV,[27] so the absorption cannot be attributed to MgO matrix. Considering the notable shift of MgO (200) diffraction peak in XRD results, the absorption in the deep-UV region can be attributed to the formation of cubic MgZnO alloys, whose band gap energy is lower than MgO. This result is consistent with the earlier reports about cubic MgZnO.[11,28]

Raman scattering spectra of the samples are collected in a backscattering geometric configuration at room temperature. The 325 nm line of a He-Cd laser is used as the excitation source. Except for the sample annealed at 1100 °C, all the samples show intense multiphonon scattering in the range from 300 to 3800 cm^{-1}. Figure 4 shows a typical resonant Raman scattering spectrum of the sample annealed at 500 °C. The Raman spectrum is composed of six sharp lines at frequency shifts that are multiples of the 1-longitudinal optical (LO) zone-center frequency of 585 cm^{-1}. This result is consistent with previously reported values of Raman shift for ZnO bulk and thin films,[29,30] which also indicates the formation of ZnO nanoparticles in these samples. In a previous report,[31] Scott and his co-workers pointed out that the number of multiple phonon-scattering processes in semiconductors varies monotonically with polaron coupling coefficient ρ, and the deformation energy is equal $\rho\hbar\omega_{LO}/2$. Then, the appearance of six Raman lines in Fig. 4 indicates that the ZnO nanoparticles embedded in MgO films have large deformation energy. Additionally, the 1-LO phonon frequency shifts to the high-energy side relative to ZnO bulk or thin films. The details are shown in the inset of Fig. 4, where the data point at 200 °C represents the as-grown sample. It is known that ZnO has hexagonal structure with $a=3.253$ Å and $c=5.213$ Å, whereas MgO has cubic structure with $a=4.213$ Å. When hexagonal ZnO nanoparticles are embedded in a cubic MgO matrix, the large mismatch between ZnO and MgO lattices must subject the ZnO nanoparticles to intense stress. Thus, the shift of 1-LO phonon frequencies can be tentatively attributed to compressive strain on the ZnO nanoparticles. As discussed previously, in the as-grown sample and the sample annealed at 300 °C, the quantity and the size of ZnO nanoparticles are small, so the interface between ZnO and MgO plays an important role in the structural properties of ZnO nanoparticles. As a result, the stress effect is remarkable in these samples. However, when annealed at higher temperature, the frequency shift of 1-LO phonon regresses to 584 cm^{-1}. The reasons for the redshift of 1-LO phonon frequency may be as follows. The strain relaxes due to the improvement of the crystal quality with increasing annealing temperature; the hexagonal MgZnO alloy layers forms between ZnO nanoparticles and MgO matrix;[32] the ZnO particle size decreases with increasing annealing temperature, which is consistent with previous reports.[33,34]

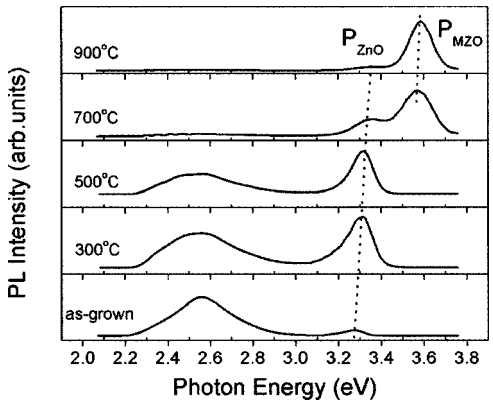

FIG. 5. PL spectra of the as-grown sample and the samples annealed at 300 °C–900 °C.

Figure 5 shows the PL spectra at room temperature for the as-grown sample and those annealed in the range from 300 °C to 900 °C. In Fig. 5, two emission bands are observed: the near-band-edge (NBE) emission in the UV region and the deep-level (DL) emission in the visible light region. The latter is typically attributable to the presence of impurities and structural defects in ZnO.[35–37] In addition, for the samples annealed at 700 °C and 900 °C, the NBE emission bands are composed of two peaks, labeled as P_{ZnO} and P_{MZO}. According to the results of XRD and optical absorption spectra, the P_{MZO} peaks at the higher energy side can be attributed to exciton emission of hexagonal MgZnO alloys, while the P_{ZnO} peaks at the lower energy side are attributed to free-exciton recombination in ZnO nanoparticles. The emissions from ZnO nanoparticles show a Stokes shift from the absorption edge and shift to the high energy side with increasing annealing temperature, which is consistent with the blueshift of the band gap in absorption spectra due to the size decrease of ZnO nano-articles. Similar to the blueshift of the absorption edge, the emissions from hexagonal MgZnO alloys are blueshifted slightly for the samples annealed at 700 °C and 900 °C, indicating the increasing Mg content in MgZnO alloy. On the other hand, the PL intensity ratio of P_{ZnO} to P_{MZO} decreases with increasing annealing temperature, which can be attributed to the depletion of ZnO for the formation of MgZnO alloys.

From Fig. 5, it can also be observed that the PL intensity ratio of UV emission band to DL band increases gradually with increasing annealing temperature, indicating the reduction of defect-state density in ZnO nanoparticles and MgZnO alloys. This can be ascribed to the improvement of crystal quality of ZnO nanoparticles and the formation of smooth interfaces among ZnO nanoparticles, MgZnO alloys, and MgO matrix with increasing annealing temperature. Since hexagonal MgZnO alloys with a lattice constant close to ZnO have formed between ZnO nanoparticles and MgO matrix by annealing samples at 500 °–900 °C, smooth interfaces between ZnO nanoparticles and hexagonal MgZnO alloys can be expected, and the surface defects of ZnO nanoparticles are efficiently passivated, resulting in a decrease of DL emissions.[38–40] However, no PL emission is observed in the sample annealed at 1100 °C, because the band gap of cubic MgZnO alloy is far beyond the excitation energy used in these PL measurements.

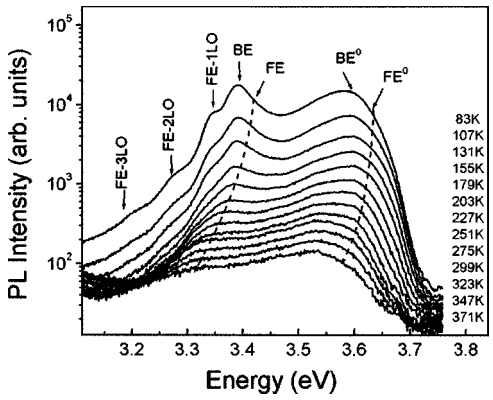

FIG. 6. Temperature-dependent PL spectra of the sample annealed at 900 °C.

Figure 6 shows the temperature-dependent PL spectra of the sample annealed at 900 °C. At 83 K, the PL spectrum is composed of a series of emission peaks. Based on the peak energies of these emission peaks, the peaks labeled as FE^0 and BE^0 can be attributed to the free-exciton and bound-exciton emissions from hexagonal MgZnO alloys, respectively. And, the peaks labeled as FE and BE are identified as the free-exciton and bound-exciton emissions of ZnO nanoparticles, while the LO-phonon replicas of FE-1LO, FE-2LO, and FE-3LO have been identified based on the energy interval between the FE peak and the LO phonon [$\hbar\omega_{\mathrm{LO}} = 72$ meV(584 cm^{-1})]. In comparison with ZnO bulk and thin films,[41] the FWHM of the PL peaks in Fig. 6 is broader, which may result from the size distribution of ZnO nanoparticles and the compositional fluctuation in MgZnO alloys. Additionally, from Fig. 6 it can be observed that all the emissions are shifted to lower energy and the PL intensities decrease gradually with increasing temperature. The bound-exciton emissions appear to be thermally quenched as the temperature exceeds 155K. Generally, the thermal quenching of luminescence intensity can be expressed as $I(T)=I_0/[1+A\exp(-E/K_BT)]$,[42] where E is the activation energy of the thermal quenching process, K_B is the Boltzmann constant, I_0 is the emission intensity at 0 K, T is the thermodynamic temperature, and A is a constant. The temperature dependence of FE^0 and FE intensities are fitted to the equation above and the activation energies are deduced to be 58 meV for FE^0 and 65 meV for FE. The activation energy of FE^0 for MgZnO alloys is comparable with the exciton binding energy, 60 meV, for ZnO bulk,[4] while the activation energy of FE for ZnO nanoparticles is 5 meV larger than 60 meV. The increase of activation energy in ZnO nanoparticles can be attributed to the small size of ZnO nanoparticles (core) and the formation of MgZnO alloys surface layer (shell) on ZnO nanoparticles, both of which contribute to the enhanced confinement of carriers in ZnO nanoparticles.

To explain the results above, the following structural description should be taken into account. For the sample annealed at 300 °C, most of the Zn nanoparticles are oxidized to ZnO nanoparticles with a small amount of residue of Zn in large-size ZnO nanoparticles, as illustrated in Fig. 7(a). As the annealing temperature increases from 500 °C to 900 °C, all Zn nanoparticles are oxidized completely to form ZnO.

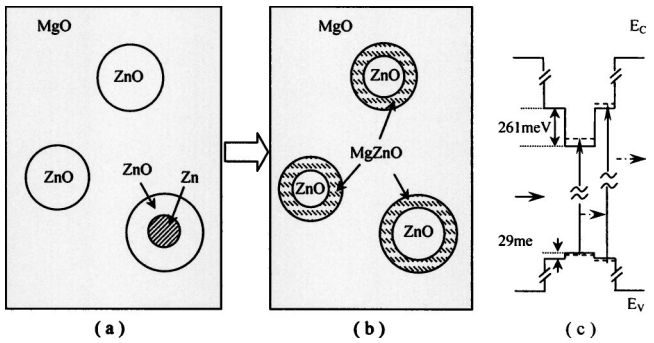

FIG. 7. Structural sketch of 300 °C (a) and 700 °C (b) annealed samples. Schematic diagram of the conduction and the valence bands of ZnO nanoparticles in 700 °C annealed sample (c).

Simultaneously, limited mutual diffusion of Mg^{2+} and Zn^{2+} between MgO matrix and ZnO nanoparticles occurs, resulting in the formation of hexagonal MgZnO alloy surface layers on the ZnO nanoparticles as illustrated in Fig. 7(b) . Figure 7(c) shows the diagram of energy bands of the sample annealed at 700 °C in which the discontinuities at the conduction and valance bands determined in Ref. 25 are used. The mean size of ZnO nanoparticles decreases with increasing annealing temperature, suggesting that the ZnO nanoparticles are gradually depleted to form MgZnO alloys. As a result, the absorption edges of ZnO nanoparticles shift to the high energy side due to the quantum confinement effects.[26,43] The increase of FE activation energy for ZnO nanoparticles, which is deduced from temperature-dependent PL spectra, can be attributed to the small size of ZnO nanoparticles and the formation of MgZnO alloys surface layer, both of which contribute to the confinement of carriers in ZnO nanoparticles. Additionally, because the annealing process promotes the diffusion of Mg^{2+} and Zn^{2+}, the Mg content increases in MgZnO alloys with increasing annealing temperature, leading to the band gap energy of hexagonal MgZnO alloys widening. When the annealing temperature is as high as 1100 °C, most zinc nanoparticles in MgO films will be reevaporated or diffuse entirely into the MgO matrix to form cubic phase MgZnO alloys. Consequently, there is no ZnO-related diffraction pattern in XRD spectrum, but an absorption in the deep-UV region.

IV. CONCLUSIONS

The structural and optical properties of ZnO nanoparticles embedded in MgO matrices were characterized by XRD, optical absorption, Raman scattering, and PL spectra. It was found that hexagonal ZnO nanoparticles and hexagonal MgZnO alloys were formed after annealing the samples at 300 °–900 °C. Additionally, annealing at 1100 °C resulted in the formation of MgZnO in cubic phase. A blueshift of the absorption edges was observed in optical absorption spectra, which was ascribed to the decrease of ZnO nanoparticle size and the formation of MgZnO alloys. The appearance of six Raman lines indicated that ZnO nanoparticles embedded in MgO matrix have large deformation energy. The big shift of 1-LO phonon frequency relative to ZnO bulk or thin films indicated that the compressive stress was significant in the as-grown sample and the sample annealed at 300 °C. In PL spectra, the UV emission bands shift to the high energy side after annealing, consistent with the results of absorption spectra.

ACKNOWLEDGMENTS

This work is supported by the Program of CAS Hundred Talents, the Key Project of National Natural Science Foundation of China under Grant No. 60336020, the National Natural Science Foundation of China under Grant Nos. 60176003, 60278031, and 60376009.

*Email address: ycliu@nenu.edu.cn

[1] D. B. Eason, Z. Yu, W. C. Hughes, W. H. Roland, C. Boney, J. W. Cook, J. F. Schetzina, G. Cantwell, and W. C. Harsch, Appl. Phys. Lett. **66**, 115 (1995).
[2] S. Nakamura, M. Senoh, S. Nagahama, N. Iwasa, T. Yamada, T. Matsushita, H. Kiyoku, and Y. Sugimoto, Jpn. J. Appl. Phys., Part 2 **35**, L217 (1996).
[3] D. C. Reynolds, D. C. Look, B. Jogai, C. W. Litton, G. Gantwell, and W. C. Harsch, Phys. Rev. B **60**, 2340 (1999).
[4] K. Hümmer, Phys. Status Solidi B **56**, 249 (1973).
[5] D. M. Bagnall, Y. F. Chen, Z. Zhu, T. Yao, S. Koyama, M. Y. Shen, and T. Goto, Appl. Phys. Lett. **70**, 2230 (1997).
[6] P. Yu, Z. K. Tang, G. K. L Wong, M. Kawasaki, A. Ohotomo, H. Koinuma, and Y. Segawa, Solid State Commun. **103**, 459 (1997).
[7] D. M. Roessler and W. C. Walker, Phys. Rev. **159**, 733 (1967).
[8] T. Bredow and R. Gerson, Phys. Rev. B **61**, 5194 (2000).
[9] A. J. Skinner and J. P. LaFemina, Phys. Rev. B **45**, 3557 (1992).
[10] T. Makino, Y. Segawa, M. Kawasaki, A. Ohtomo, R. Shiroki, K. Tamura, T. Yasuda, and H. Koinuma, Appl. Phys. Lett. **78**, 1237 (2001).
[11] A. Naraya, K. Sharma, A. Kvit, C. Jin, J. F. Muth, and O. W. Hollan, Solid State Commun. **121**, 9 (2002).
[12] K. Sakurai, T. Takagi, T. Kubo, D. Kajita, T. Tanabe, H. Takasu, S. Fujita, and S. Fujita, J. Cryst. Growth **237-239**, 514 (2002).
[13] H. D. Sun, T. Makino, N. T. Tuan, Y. Segawa, M. Kawasaki, A. Ohtomo, K. Tamura, and H. Koinuma, Appl. Phys. Lett. **78**, 2464 (2001).
[14] H. Yan, R. He, J. Johnson, M. Law, R. J. Saykally, and P. Yang, J. Am. Chem. Soc. **125**, 4728 (2003).
[15] H. Q. Yan, R. R. He, J. Pham, and P. D. Yang, Adv. Mater. (Weinheim, Ger.) **15**, 402 (2003).
[16] M. H. Huang, S. Mao, H. Feick, H. Yan, Y. Wu, H. Kind, E. Weber, R. Russo, and P. Yang, Science **292**, 1897 (2001).
[17] X. Zhao, M. Willander, R. E. Morjan, Q-H. Hu, and E. E. B. Campbell, Appl. Phys. Lett. **83**, 165 (2003).
[18] L. Guo, S. H. Yang, C. L. Yang, P. Yu, J. N. Wang, W. K. Ge, and G. Wong, Appl. Phys. Lett. **76**, 2901 (2000).

[19] W. Kern, *Handbook of Semiconductor Wafer Cleaning Technology — Science, Technology, and Applications* (William Andrew, Noyes, 1993).
[20] B. D. Cullity, *Elements of X-Ray Diffractions* (Addison-Wesley, Reading. MA, 1978), p. 102.
[21] J. Gong, W. Liao, S. Hsieh, P. Lin, and Y. Tsai, J. Cryst. Growth **249**, 28 (2003).
[22] D. X. Zhao, Y. C. Liu, D. Z. Shen, J. Y. Zhang, Y. M. Lu, and X. W. Fan, J. Cryst. Growth **249**, 163 (2003).
[23] J. M. Pawlikowski, Phys. Rev. B **26**, 4711 (1982).
[24] K. Sharma, J. Naryana, J. F. Muth, C. W. Teng, C. Jin, A. Kvit, R. M. Lkolbas, and O. W. Holland, Appl. Phys. Lett. **75**, 3327 (1999).
[25] T. Makino, C. H. Chia, Nguen T. Tuan, H. D. Sun, Y. Segawa, M. Kawasaki, A. Ohtomo, K. Tamura, and H. Koinuma, Appl. Phys. Lett. **77**, 975 (2000).
[26] W. Yang, R. D. Vispute, S. Choopun, R. P. Sharma, T. Venkatesan, and H. Shen, Appl. Phys. Lett. **78**, 2787 (2001).
[27] T. Bredow and R. Gerson, Phys. Rev. B **61**, 5194 (2000).
[28] R. Segnit and A. E. Holland, J. Am. Ceram. Soc. **48**, 412 (1965).
[29] J. F. Scott, Phys. Rev. B **2**, 1209 (1970).
[30] X. T. Zhang, Y. C. Liu, L. G. Zhang, J. Y. Zhang, Y. M. Lu, D. Z. Shen, W. Xu, G. Z. Zhong, X. W. Fan, and X. G. Kong, J. Appl. Phys. **92**, 3293 (2002).
[31] J. F. Soctt, T. C. Damen, W. T. Silfvast, R. C. C. Leite, and L. E. Cheesman, Opt. Commun. **1**, 397 (1970).
[32] R. D. Shannon, Acta Crystallogr., Sect. A: Cryst. Phys., Diffr., Theor. Gen. Crystallogr. **32**, 751 (1976).
[33] M. Rajalakshmi, A. K. Arora, B. S. Bendre, and S. Mahamuni, J. Appl. Phys. **87**, 2445 (2000).
[34] Al. L. Efros, A. I. Ekimov, F. Kozlowski, V. Petrova-Koch, H. Schmidbaur, and S. Shumilov, Solid State Commun. **78**, 853 (1991).
[35] K. Vanheusden, W. L. Warren, C. H. Seager, D. R. Tallant, J. A. Voigt, and B. E. Gnade, J. Appl. Phys. **79**, 7983 (1996).
[36] J. W. Hu and Y. Bando, Appl. Phys. Lett. **82**, 1401 (2003).
[37] S. A. Studenikin and M. Cocivera, J. Appl. Phys. **91**, 5060 (2002).
[38] D. C. Reynolds, D. C. Look, and B. Jogai, J. Appl. Phys. **89**, 6189 (2001).
[39] D. Yao, Y. F. Chan, and N. Wang, Appl. Phys. Lett. **81**, 757 (2002).
[40] S. Monticone, R. Tufeu, and A. M. Kanaev, J. Phys. Chem. B **102**, 2854 (1998).
[41] D. W. Hamby, D. A. Lucca, M. J. Klopfstein, and G. Cantwell, J. Appl. Phys. **93**, 3214 (2003).
[42] P. O. Holtz, B. Monemar, and H. J. Lozykowski, Phys. Rev. B **32**, 986 (1985).
[43] L. E. Brus, J. Chem. Phys. **80**, 4403 (1984).